



Optimization of Contrast to Tissue Ratio by Frequency Adaptation in Pulse Inversion Imaging

Sébastien Ménigot, Jean-Marc Girault, Iulian Voicu, Anthony Novell

► To cite this version:

Sébastien Ménigot, Jean-Marc Girault, Iulian Voicu, Anthony Novell. Optimization of Contrast to Tissue Ratio by Frequency Adaptation in Pulse Inversion Imaging. IEEE Transactions on Ultrasonics, Ferroelectrics and Frequency Control, Institute of Electrical and Electronics Engineers, 2012, 59 (11), pp.2431-2438. <10.1109/TUFFC.2012.2475>. <hal-00731343>

HAL Id: hal-00731343

<https://hal.archives-ouvertes.fr/hal-00731343>

Submitted on 21 Nov 2012

HAL is a multi-disciplinary open access archive for the deposit and dissemination of scientific research documents, whether they are published or not. The documents may come from teaching and research institutions in France or abroad, or from public or private research centers.

L'archive ouverte pluridisciplinaire **HAL**, est destinée au dépôt et à la diffusion de documents scientifiques de niveau recherche, publiés ou non, émanant des établissements d'enseignement et de recherche français ou étrangers, des laboratoires publics ou privés.

Optimization of Contrast to Tissue Ratio by Frequency Adaptation in Pulse Inversion Imaging

Sébastien Ménigot, Jean-Marc Girault, *Member, IEEE*, Iulian Voicu,
and Anthony Novell, *Member, IEEE*

Abstract

Contrast imaging has significantly improved clinical diagnosis by increasing the contrast-to-tissue ratio after microbubble injection. Pulse inversion imaging is the most commonly used contrast imaging technique, as it greatly increases the contrast-to-tissue ratio by extracting microbubble nonlinearities. The main purpose of our study was to propose an automatic technique providing the best contrast-to-tissue ratio throughout the experiment. For reasons of simplicity, we proposed to maximize the contrast-to-tissue ratio with an appropriate choice of the transmit frequency. The contrast-to-tissue ratio was maximized by a closed loop system including the pulse inversion technique. An algorithm based on the gradient provided iterative determination of the optimal transmit frequency. The optimization method converged quickly after six iterations. This optimal control method is easy to implement and it optimizes the contrast-to-tissue ratio by selecting the transmit frequency adaptively.

Index Terms

Adaptive system, closed loop system, contrast enhancement, microbubbles, optimal control, optimization, pulse inversion technique, signal processing, transmitted pulse, ultrasound imaging.

Manuscript received November 21, 2012. The authors thank the Agence Nationale de la Recherche (Projects ANR-07-TECSAN-015 MONITHER and ANR-07-TECSAN-023 SURFOETUS) for financial support.

The authors are with Université François-Rabelais de Tours, UMR-S930, Tours, France. They are also with Inserm, U 930, Tours, France (e-mails: sebastien.menigot@univ-tours.fr, jean-marc.girault@univ-tours.fr).

©2012 IEEE. Reprinted, with permission, from Sébastien Ménigot, Jean-Marc Girault, Iulian Voicu and Anthony Novell, Optimization of Contrast to Tissue Ratio by Frequency Adaptation in Pulse Inversion Imaging, IEEE Transactions on Ultrasonics Ferroelectrics and Frequency Control, Nov. 2012]. This material is posted here with permission of the IEEE. Such permission of the IEEE does not in any way imply IEEE endorsement of any of the Université François Rabelais de Tours' products or services. Internal or personal use of this material is permitted. However, permission to reprint/republish this material for advertising or promotional purposes or for creating new collective works for resale or redistribution must be obtained from the IEEE by writing to pubs-permissions@ieee.org.

I. INTRODUCTION

OVER the past twenty years, improvements in the sensitivity of medical ultrasound imaging systems have provided more accurate medical diagnoses through intravenous injection of ultrasound contrast agents containing microbubbles. The perfusion imaging thus obtained, as in the myocardium or in tumors for example, has provided physiological and pathological information [1]. Initially, the linear interactions between the microbubbles and the ultrasound waves were only operated in B-mode, to increase the sensitivity between the tissue and the microbubbles. However, the use of ultrasound contrast imaging was revolutionized in clinical practice when the nonlinear interaction was taken into account. The nonlinearity of contrast agent responses has become a major focus of research to obtain the best contrast-to-tissue ratio (*CTR*). However, obtaining an ideal method has been limited by two factors. First, good separation of the harmonic components requires a limited pulse bandwidth [2], which reduces the axial resolution as in second harmonic imaging [3], and secondly the effects of the ultrasound wave propagation limit the *CTR* because of the presence of nonlinear components generated in tissue [1].

Several imaging methods have been proposed to improve *CTR* and/or resolution. Some of the best known techniques such as second harmonic imaging [3], subharmonic imaging [4], super harmonic imaging [5], imaging using second order Volterra filter [6] and attenuation correction [7] have been mainly based on post-processing. Some techniques have been based on post-processing with discrete or continuous encoding of the amplitude, the phase or the frequency of the transmitted ultrasound wave. They use differences in nonlinear acoustic signatures of microbubbles and tissue, such as pulse inversion [8], power modulation [9], contrast pulse sequencing [10], pulse subtraction [11] and harmonic chirp imaging [12].

The setting parameters must be correctly adjusted for optimal use of these methods. However, there is usually no optimization process, the pulse settings to date being manual and pre-selected. The aim of the study presented here was to find the setting parameters of the technique to be used to provide the best *CTR*, the best resolution or the best compromise between *CTR* and resolution. This step is crucial. Unfortunately, solution of the problem often requires *a priori* knowledge of the medium and transducer that is inaccessible. Moreover, the existing methods cannot adjust to different variations throughout a qualitative medical examination, as may be the case for a variation in microbubble concentration [13] or microbubble size [14]. No method has been able to solve this problem to date.

In this study, we aimed to solve this problem through the concept of the optimal command: the system

parameters θ were set by optimizing a cost function J (e.g. the CTR):

$$\theta^* = \arg \max_{\theta} (J(\theta)), \quad (1)$$

where θ^* are the optimal system parameters. We therefore replaced the current system with a closed loop system whose transmitted pulse was modified by feedback. Implementation of optimization required two steps: specification of the cost function J and specification of the setting parameters θ .

In the first step, the cost function J was chosen to take into account the user's needs and the medical application. Here, in contrast harmonic imaging, the cost function was the CTR . This choice was also justified by the microbubble sensitivity of the CTR . Moreover, to complement our approach, microbubble detection was performed by pulse inversion imaging [8], since it is one of the most common methods used to increase CTR while ensuring good axial resolution.

In the second step, the CTR optimization must be achieved without *a priori* knowledge of the imaging system [15] (i.e. explored medium, the transducer and pulse parameters), since such information is inaccessible in practice. As we wanted to optimize the CTR by modifying the signal transmitted, we could propose adjusting parameters characterizing the transmitted signal such as frequency, amplitude, phase or pulse duration. It should be noted that both the amplitude and the frequency are relevant pulse parameters which contribute to a significant increase in microbubble response, as in the case of power modulation or chirp imaging, respectively. To simplify our approach, we therefore chose to optimize only the transmit frequency f , for a pulse inversion imaging system, thereby producing a new device that can adapt to changing conditions.

Consequently, the optimization problem can be written as follows:

$$f^* = \arg \max_f (CTR(f)), \quad (2)$$

where f^* is the optimal transmit frequency which provides the best CTR . We proposed an iterative approach to find the optimal transmit frequency f^* and we applied it in simulations and in experiment.

II. CLOSED-LOOP IMAGING SYSTEM

The principle of pulse inversion imaging including feedback is described in Fig. 1. At the iteration k , two pulses $x_{k,1}(t)$ and $x_{k,2}(t)$ with opposite phases and with a frequency f_k were transmitted. The sum

67 $z_k(t)$ of the two respective echoes $y_{k,1}(t)$ and $y_{k,2}(t)$ formed a radiofrequency line of the image I_k . From
 68 the CTR_k measured on this image I_k , a new transmit frequency f_{k+1} was computed by the algorithm to
 69 optimize the CTR_{k+1} on the next image I_{k+1} .

70 [Fig. 1 about here.]

71 A. Transmitted Signal

72 The pulse signal $x_{k,p}(t)$ at transmit frequency f_k was computed digitally with Matlab (Mathworks,
 73 Natick, MA, USA):

$$x_{k,p}(t) = A \cdot w_{k,p}(t). \quad (3)$$

74 The sinus modulated by a Gaussian function [12] $w_{k,p}(t)$ was constructed as follows:

$$w_{k,p}(t) = \exp \left[-\frac{(t - t_0)^2}{\frac{N_c}{2f_k}} \right] \sin(2\pi f_k t + \phi_p), \quad (4)$$

75 where t is the time, t_0 the time for which the Gaussian function is maximum, N_c the cycle number and
 76 ϕ_p the phase equal to 0° if $p = 1$ and π if $p = 2$.

77 The amplitude of the driving pressure A was then adjusted so that the power of the pulse $x_{k,p}(t)$ was
 78 constant for all iterations:

$$A = \sqrt{\frac{A_0^2 \cdot P_{x_{ref}}}{P_w}}, \quad (5)$$

79 where A_0 is the driving pressure amplitude of the reference signal x_{ref} . This signal x_{ref} was calculated
 80 at the central frequency of the transducer. Its power $P_{x_{ref}}$ constituted the reference power, while P_w was
 81 the power of the signal $w_{k,p}$. The power of the transmitted wave thus remained constant by adjusting the
 82 amplitude signal A .

83 B. Cost Function

84 In the receiver, CTR_k was computed from a line $z_k(t)$ of pulse inversion image:

$$z_k(t) = y_{k,1}(t) + y_{k,2}(t), \quad (6)$$

85 where $y_{k,p}(t)$ is the echo of the transmitted pulse $x_{k,p}(t)$. It is defined as the ratio of the power $P_{b,k}$
 86 backscattered by the area of the perfused medium to the power $P_{t,k}$ backscattered by the area of the
 87 non-perfused medium [6] as follows:

$$CTR_k = 10 \cdot \log_{10} \left(\frac{P_{b,k}}{P_{t,k}} \right), \quad (7)$$

88 These powers were measured from the lines $z_k(t)$ of the pulse inversion image at iteration k . The areas
 89 were determined manually before the optimization process, but a segmentation step could be implemented.

90 The contrast gain G_{dB} was also defined between the optimized system and the non-optimized system.
 91 The CTR obtained with the non-optimized system was determined at the central frequency of the
 92 transducer [16]. The contrast gain G_{dB} is obtained by the next equation:

$$G_{dB} = \frac{CTR(f^*)}{CTR(f_0)}, \quad (8)$$

93 where $CTR(f_0)$ is the CTR obtained at the central frequency of the transducer.

94 C. Iterative Optimization Algorithm

95 The algorithm was based on the principle of the gradient descent [17]. It determined a new transmit
 96 frequency f_{k+1} for the next pulse sequence to optimize the CTR_{k+1} by the following recurrence relation:

$$f_{k+1} = f_k + \mu_k \cdot d_k, \quad (9)$$

97 The first coefficient μ_k set the speed of convergence as follows:

$$\mu_k = \begin{cases} 0 & \text{if } k \leq 3; \\ \Delta f & \text{if } k = 4; \\ \mu_{k-1} & \text{if } \text{sgn}(\nabla CTR(f_k)) = \text{sgn}(\nabla CTR(f_{k-1})); \\ \frac{\mu_{k-1}}{2} & \text{if } \text{sgn}(\nabla CTR(f_k)) \neq \text{sgn}(\nabla CTR(f_{k-1})). \end{cases} \quad (10)$$

98 where Δf fixed at 100 kHz provided the best compromise between speed of convergence and robustness,
 99 the sign function $\text{sgn}(t)$ is equal to 1 if $t > 0$, 0 if $t = 0$ and -1 if $t < 0$, and the CTR gradient defined

100 by:

$$\nabla CTR(f_k) = \frac{CTR_k - CTR_{k-1}}{f_k - f_{k-1}}. \quad (11)$$

101 The second coefficient d_k set the direction as follows:

$$d_k = \begin{cases} 1 & \text{if } k \leq 3; \\ 1 & \text{if } \text{sgn}(\nabla CTR(f_k)) = \text{sgn}(\nabla CTR(f_{k-1})); \\ -1 & \text{if } \text{sgn}(\nabla CTR(f_k)) \neq \text{sgn}(\nabla CTR(f_{k-1})). \end{cases} \quad (12)$$

102 In order to compute μ_k and d_k , the system operated in open loop for the first three iterations ($k =$
 103 $\{1, 2, 3\}$). The first three frequencies f_1 , f_2 and f_3 were chosen initially. The appropriate choice could
 104 increase the speed of convergence, but it was not essential to reach the optimal CTR , when the cost
 105 function was concave.

106 III. SIMULATION EVALUATION

107 The optimization principle was initially applied in simulation. Several simulations were performed to
 108 demonstrate the feasibility of our novel method.

109 A. Simulation Model

110 The simulation model followed the same process as described in the experimental setup (Fig. 1). It was
 111 composed of different phases: transmission, 2D nonlinear forward propagation, nonlinear oscillations
 112 of microbubbles, 2D nonlinear backward propagation and reception. A pulse wave was nonlinearly
 113 propagated into an attenuating intermediate medium without microbubbles. This wave, composed of
 114 harmonic components, excited a microbubble in the vascular system. The nonlinear oscillations of this
 115 microbubble were backscattered and measured by the receiver.

116 *1) Nonlinear Propagation in Tissue:* The core of the model was based on the free simulation program
 117 developed by Anderson [18], and *e.g.*, used in [19]. It consisted of digitally solving the 2D nonlinear
 118 wave propagation into an attenuating medium by using a pseudo-spectral derivative and a time-domain
 119 integration algorithm.

120 A pulse signal was generated digitally at iteration k and filtered by the transfer function of the ultrasound
 121 probe used in the experiment, centred at 4 MHz with a fractional bandwidth of 53% at -3 dB. Here, to

reduce the computation time, only 8 elements of the ultrasound probe composed of 128 elements were used. Note that linear beamforming was used in transmission and in reception [20] so that the beam was focused at 15 mm from the transducer. The nonlinear wave propagation into the intermediate medium was obtained by solving Anderson's model where the physical parameters were the following [20]:

- density of $928 \text{ kg}\cdot\text{m}^{-3}$;
- speed of sound of $1578 \text{ m}\cdot\text{s}^{-1}$;
- B/A nonlinearity parameter of 6.7;
- attenuation of $0.45 \text{ dB}\cdot\text{MHz}^{-1.05}\cdot\text{cm}^{-1}$.

This driving pressure at the focus point was included into the microbubble model described below. Finally, the wave backscattered by the microbubble was nonlinearly backpropagated up to the receiver. This signal was filtered by the transfer function of the same ultrasound probe used in experiment. To take into account imperfections in our simulation, a white noise $\varepsilon(t)$ was added to $x_{k,p}(t)$, and a signal-to-noise ratio (SNR) of 50 dB was chosen.

2) *Microbubble*: The simulated ultrasound contrast agent had the properties of encapsulated microbubbles of SonoVue (Bracco Research SpA, Geneva, Switzerland), with a phospholipid monolayer imprisoning sulfur hexafluoride gas (SF_6) [21] where the polytropic gas exponent κ was 1.095. The microbubbles had the following properties:

- mean diameter: $2.5 \text{ }\mu\text{m}$ [21];
- resonance frequency: 2.6 MHz [22].

The acoustic response was computed for one microbubble from the model of Marmottant [23] based on the Rayleigh-Plesset equation [24] and the polytropic transformation. The solver used was the fourth-order Runge-Kutta method. Finally the surface pressure of the microbubble was transmitted to the nonlinear propagation model in order to deduce the backscattered signal. In order to simulate the mean behavior of a microbubble cloud, we hypothesized that the response of a cloud of N microbubbles was N times the response of a single microbubble with the mean properties. To be more realistic, the attenuation effects due to the high concentration of microbubbles were taken into account [25] for a dilution of $1/2000$.

B. Simulation Results

1) *Empirical Optimization*: Fig. 2 represents the results of the first simulation, *i.e.* the *CTR* as a function of the transmit frequency for different pressure levels A_0 (from 240 to 400 kPa). The number of

cycles N_c was set at 2.3 cycles so that the relative bandwidth¹ was 100% at the central frequency of the transducer.

The first results indicated that the CTR had a global maximum whatever the pressure level A_0 , and showed that the CTR can be improved by choosing the appropriate transmit frequency, thus confirming the validity of our study. This property could be also interesting, because an automatic search could more easily be achieved by a gradient algorithm. The second result demonstrated that the higher the pressure, the higher the global maximum of the CTR , because the power backscattered by the microbubble increased more quickly than the power backscattered by the tissue particle when the pressure level increased. The maximum values of the CTR ranged between 21.2 dB and 22.2 dB for pressure levels A_0 ranging from 240 to 400 kPa, and the contrast gain G_{dB} was from 14.3 to 9.1 dB, respectively. These results revealed that the best transmit frequency was not the central frequency of the transducer, again confirming the need to optimize the imaging process.

To summarize, the results shown in Fig. 2 confirmed the need to optimize the imaging system by seeking the best transmit frequency which maximized the CTR function. Indeed, Fig. 2 shows that the CTR depended on transmit frequency f and could reach a single global maximum of approximately 22 dB. The single maximum of the CTR could be detected automatically by a simple technique such as the gradient. Note that the optimal transmit frequency was lower than the transmit frequency which produced the best axial resolution.

[Fig. 2 about here.]

2) *Automatic Optimization:* The maximum CTR was reached automatically using the gradient algorithm. Fig. 3b shows the CTR measured at each iteration k , and Fig. 3a shows variations in the transmit frequency during iterations.

The transmit frequency converged to a stable value after six iterations, whatever the pressure level A_0 . As an illustration, the black solid line in Fig. 2 shows the first twenty iterations which confirmed the convergence after the first six iterations. Moreover, the CTR reached its maximum when the transmit frequency converged. Note that the CTR and the contrast gain G_{dB} obtained automatically were equal to those obtained empirically in the first simulation.

As depicted in Fig. 2, the optimal transmit frequency was lower than the central frequency of the transducer. Moreover, this optimal transmit frequency was equal to neither the central frequency of the

¹The relative bandwidth was defined as the percentage of the bandwidth of the signal in the fractional bandwidth of the transducer.

transducer nor to the microbubble resonance frequency. However, this optimal transmit frequency obtained after convergence of the algorithm made it possible to receive the harmonic components necessary to optimize the *CTR*.

In summary, the results in Fig. 3 show that it was possible to find the transmit frequency which maximized the *CTR* automatically. No *a priori* knowledge was required, except for the choice of the first three transmit frequencies which impacted on the speed of convergence.

[Fig. 3 about here.]

3) *Adaptive Optimization*: Fig. 4 depicts the *CTR* and the transmit frequency as a function of iterations when:

- 1) the microbubble radius was fixed at $2.5 \mu\text{m}$ throughout the simulation;
- 2) the microbubble radius was fixed at $1.25 \mu\text{m}$ throughout the simulation;
- 3) the microbubble radius decreased with time, increasing its linear resonance frequency. In the simulation, the radius changed from 2.5 to 1.25 at iteration 10.

The results showed that the first optimization (*i.e.* with a microbubble of $2.5 \mu\text{m}$) converged at a transmit frequency of 1.9 MHz for a *CTR* of 22.1 dB . The second optimization converged at a transmit frequency of 2.1 MHz for a *CTR* of 16.6 dB . For the third optimization, the values of the *CTR* converged to the previously obtained values. Our system provided a quasi-instantaneous adaptation of the *CTR* during simulation. In all three simulations, convergence was reached after ten iterations. Note that the optimal transmit frequency was different for different sizes of microbubbles. Furthermore, when the oscillations increased as the size of the microbubble increased and thus the backscattered power increased. Hence, the *CTR* was dependent on the microbubble size.

To summarize, our optimization method adjusted the transmit frequency throughout the simulation by taking into account the changes in the microbubble properties. When the contrast agent did not change, the *CTR* did not change. This adaptability was also demonstrated when the tissue or the transducer changed with time. Note that when the optimization was not quick or robust enough, another algorithm could be used. However, for the gradient algorithm, the speed of convergence could enable us to reset the optimization parameter μ_k if the environment changed a great deal.

[Fig. 4 about here.]

208 4) *Note on Resolution:* In the previous results, the axial resolution varied with the transmit frequency
 209 since the number of cycles N_c was constant. An alternative solution can ensure a constant axial resolution
 210 if the variations in transmit frequency are compensated for by changing the number of cycles $N_c(k)$ for
 211 each iteration k . The length of the pulse $x_{k,p}(t)$ thus remained constant whatever the transmit frequency
 212 as follows:

$$2\sigma_t(k)^2 = \frac{N_c(k)}{2f_k} = \text{constant}, \quad (13)$$

213 where $2\sigma_t(k)^2$ is the pulse duration at iteration k . In this case, when f_k decreased, $N_c(k)$ decreased.
 214 When the axial resolution was 100% of the relative bandwidth (*i.e.* 0.45 mm), the maximum values of
 215 CTR ranged between 17.9 dB and 19.8 dB for pressure levels A_0 increasing from 240 to 400 kPa, and
 216 the contrast gains G_{dB} ranged between 10.9 and 6.6 dB. Note that the CTR and the gain were smaller
 217 with this setting compared to the previous results when N_c was constant. Indeed, the small number of
 218 cycles reduced the good separation of harmonic components. Consequently, increasing the axial resolution
 219 reduced the CTR . Finally, the system converged at the maximum CTR with the same speed of convergence
 220 as indicated by Fig. 3.

221 IV. EXPERIMENTAL VALIDATION

222 The aim of this section was to confirm experimentally the results obtained in the simulation.

223 A. Experimental Setup

224 The experimental setup is presented in Fig. 1. The signals transmitted ($x_{k,1}(t)$ and $x_{k,2}(t)$) were first
 225 generated digitally by a personal computer using equation 3. They were sent from an ultrasound scanner
 226 to the medium via an ultrasound probe. The waves insonified the medium which was composed of tissues
 227 and microbubbles. The reception system collected the echoes $y_{k,1}(t)$ and $y_{k,2}(t)$ and computed a pulse
 228 inversion image line.

229 1) *Ultrasound Scanner and Transducers:* The transmitted signal $x_{k,p}(t)$ was sent to an “open”
 230 ultrasound scanner (MultiX WM, M2M, Les Ulis, France). This ultrasound scanner automatically
 231 duplicated the signal $x_{k,p}(t)$ for each element of the ultrasound probe. It applied the delays necessary
 232 to obtain phased-array beamforming [20]. Then the signals were transmitted to a linear array of 128

elements (Vermon SA, Tours, France), centred at 4 MHz with a fractional bandwidth of 53% at -3 dB. The beam was focused at 28 mm from the surface.

The pulse transfer time for a single focusing was high, because it took approximately two seconds per radio frequency line. Consequently, we proposed optimization carried out only on an ultrasound image of five lines sweeping an angle of $0^\circ 25'$. The duration of the experiment was reduced to limit microbubble destruction.

2) *Medium Explored*: The wave propagated through a tissue-mimicking phantom (model 524, peripheral vascular Doppler flow phantom, ATS Laboratories Inc, Bridgeport, CT, USA), crossed by a 4 mm-diameter tube in which a 1/2000 diluted solution of SonoVue circulated.

The pulse was chosen with a cycle number corresponding to 55% of the relative bandwidth at the central frequency of the transducer (*i.e.* $N_c = 4$) and with a pressure level A_0 of 400 kPa at the focal point.

B. Experimental Results

The experimental results presented in Fig. 5 show the transmit frequency and the *CTR* during the iterations. Fig. 5b shows that the *CTR* converged to its optimal value after six iterations. The mean *CTR* achieved after convergence was around 12.22 dB ± 2.4 dB, *i.e.* a mean contrast gain of 7.77 dB. Fig. 5a shows that the transmit frequency converged to 2.9 MHz ± 0.1 MHz. The temporal fluctuation of the transmit frequency showed that the system adjusted itself to changes. These variations may have been caused by two effects: (i) statistical fluctuation due to microbubble movements and (ii) fluctuation related to changes in the size distribution of microbubbles and number of microbubbles. However, these results did not permit definitive conclusion regarding the nature of the fluctuation and we could only conclude that our system automatically adjusted itself.

[Fig. 5 about here.]

Furthermore, the experimental results were in accordance with our simulation results: we observed that the optimal transmit frequency was lower than the central frequency of the transducer. This optimal transmit frequency obtained after the algorithm convergence also made it possible to receive the harmonic components required in the *CTR* optimization. Note that the difference between the gain value in our simulation and that obtained in our experiment might be due to the more simplistic hypothesis of the model used.

Finally, these experimental results confirmed the feasibility of our method.

V. DISCUSSION AND CONCLUSIONS

CTR optimization in pulse inversion imaging was performed automatically, without taking into account *a priori* knowledge of the medium or the transducer, except for the first three values of the transmit frequency chosen only for their impact on the speed of convergence. The optimal transmit frequency was reached automatically by feedback within only a few iterations. The algorithm itself adjusted the transmit frequency throughout the experiment by each time taking into account the changes in microbubble properties. This closed loop system gave the best compromise between the transducer bandwidth and the frequency responses of microbubbles and tissue. This trade-off has usually been calculated empirically to date. To make such automatic trade-off possible, the proposed algorithm itself adjusted the transmit frequency to maximize the power backscattered by microbubbles while minimizing the power backscattered by the tissue within the transducer bandwidth.

Our method was feasible for two reasons. Optimization was iteratively fulfilled by using (i) an easily implemented algorithm and (ii) a single setting parameter (here the transmit frequency). One major advantage of our approach was that it adjusted itself to any medium explored by taking into account the effects of attenuation and nonlinear propagation. This advantage was due to the fact that the cost function, on which the optimization was based, was exclusively the result of the input and the output measurements of our system. One interesting consequence is that our method can be applied to any imaging system and to any medium to be explored, since our algorithm should converge to the maximum of the cost-function. Note that for a robust optimization, this maximum must be exclusive.

We identified three major points for discussion, for future integration in an imaging system:

- the first concerned the gradient algorithm for which six basic operations were necessary to compute the transmit frequency for the next iteration. This low number of operations should not significantly change the frame rate;
- the second concerned the *CTR* computation from regions of interest ($L \times L$ size) in the image of size $M \times M$. For efficient optimization, it is important to determine the correct positions of the perfused and non-perfused areas. Indeed, poor assessment of the *CTR* could lead to poor optimization. Moreover, the *CTR* computation required $2(2L+1)^2+1$ operations. It should not considerably change the frame rate;

- the third concerned the transfer time between the computer and the programmable analogue transmitter. Note that for our “open” ultrasound scanner, this transfer time was not negligible compared to the frame rate. Indeed, this had led us to limit the image size. However we do not think that is is a problem for future integration of our method in an imaging system, since the current development of new imaging methods based on chirp or time reversal also requires such instrumentation.

Finally, our method only focused on qualitative imaging. Although our technique could offer an optimal frequency for each image line, it was preferable to perform optimization on the whole image, because the image had a single resolution. For instance, our optimization without resolution constraints could offer the best tradeoff between the *CTR* and axial resolution. We therefore believe that the method would be particularly appropriate for contrast echocardiography where the tradeoff must favor contrast [3]. Nevertheless, our method was suitable for quantitative contrast ultrasound imaging, since it adjusted itself to microbubble variations, although a possible solution may be to cease optimization during the quantification step.

To conclude, the method ensured optimal *CTR* throughout the experiments by adaptively selecting the transmit frequency. With our new approach, manufacturers and clinicians would not themselves need to tune the transmit frequency. The method should automatically adapt the transmit frequency to the medical examination conditions and maintain optimal *CTR*. Finally, our closed-loop method should be adapted using a larger number of contrast imaging techniques.

ACKNOWLEDGEMENTS

The authors would like to thank A. Zaylaa and A. Bouakaz for helpful discussions and for language editing of the manuscript, and the Clinical Investigation Centre for Innovative Technology of Tours (CIC-IT 806 CHRU de Tours, Tours, France) for the ultrasound contrast agents.

The authors would also like to thank the anonymous reviewers for their valuable comments.

REFERENCES

- [1] P. J. A. Frinking, A. Bouakaz, J. Kirkhorn, F. J. Ten Cate, and N. de Jong, "Ultrasound Contrast Imaging: Current and New Potential Methods," *Ultrasound Med. Biol.*, vol. 26, no. 6, pp. 965–975, Jul. 2000.
- [2] M. A. Averkiou, "Tissue Harmonic Imaging," in *Proc. IEEE Ultrason. Symp.*, vol. 2, 2000, pp. 1563–1572.
- [3] P. N. Burns, "Instrumentation for Contrast Echocardiography," *Echocardiography*, vol. 19, no. 3, pp. 241–258, Apr. 2002.
- [4] F. Forsberg, W. T. Shi, and B. B. Goldberg, "Subharmonic Imaging of Contrast Agents," *Ultrasonics*, vol. 38, no. 1-8, pp. 93–98, Mar. 2000.
- [5] A. Bouakaz, S. Frigstad, F. J. Ten Cate, and N. de Jong, "Super Harmonic Imaging: A New Imaging Technique for Improved Contrast Detection," *Ultrasound Med. Biol.*, vol. 28, no. 1, pp. 59–68, Jan. 2002.
- [6] P. Phukpattaranont and E. S. Ebbini, "Post-Beamforming Second-Order Volterra Filter for Pulse-Echo Ultrasonic Imaging," *IEEE Trans. Ultrason., Ferroelectr., Freq. Control*, vol. 50, no. 8, pp. 987–1001, Aug. 2003.
- [7] M.-X. Tang, J.-M. Mari, P. N. T. Wells, and R. J. Eckersley, "Attenuation Correction in Ultrasound Contrast Agent Imaging: Elementary Theory and Preliminary Experimental Evaluation," *Ultrasound Med. Biol.*, vol. 34, no. 12, pp. 1998–2008, Dec. 2008.
- [8] D. H. Simpson, C. T. Chin, and P. N. Burns, "Pulse Inversion Doppler: A New Method for Detecting Nonlinear Echoes from Microbubble Contrast Agents," *IEEE Trans. Ultrason., Ferroelectr., Freq. Control*, vol. 46, no. 2, pp. 372–382, Mar. 1999.
- [9] G. A. Brock-fisher, M. D. Poland, and P. G. Rafter, "Means for Increasing Sensitivity in Non-linear Ultrasound Imaging Systems," U.S. Patent 5 577 505, Nov., 1996.
- [10] P. Phillips and E. Gardner, "Contrast-Agent Detection and Quantification," *Eur. Radiol.*, vol. 14, pp. 4–10, Oct. 2004.
- [11] J. M. G. Borsboom, A. Bouakaz, and N. de Jong, "Pulse Subtraction Time Delay Imaging Method for Ultrasound Contrast Agent Detection," *IEEE Trans. Ultrason., Ferroelectr., Freq. Control*, vol. 56, no. 6, pp. 1151–1158, Jun. 2009.
- [12] J. M. G. Borsboom, C. T. Chin, A. Bouakaz, M. Versluis, and N. de Jong, "Harmonic Chirp Imaging Method for Ultrasound Contrast Agent," *IEEE Trans. Ultrason., Ferroelectr., Freq. Control*, vol. 52, no. 2, pp. 241–249, Feb. 2005.
- [13] H. Becher and P. N. Burns, *Handbook of Contrast Echocardiography : Left Ventricular Function and Myocardial Perfusion*. New York, USA: Springer, 2000.
- [14] K. Soetanto and M. Chan, "Study on the Lifetime and Attenuation Properties of Microbubbles Coated with Carboxylic Acid Salts," *Ultrasonics*, vol. 38, no. 10, pp. 969–977, Nov. 2000.
- [15] S. Ménigot, A. Novell, A. Bouakaz, and J.-M. Girault, "Improvement of the Power Response in Contrast Imaging with Transmit Frequency Optimization," in *Proc. IEEE Ultrason. Symp.*, 2009, pp. 1–4.
- [16] Q. Ma, Y. Ma, X. Gong, and D. Zhang, "Improvement of Tissue Harmonic Imaging using the Pulse-Inversion Technique," *Ultrasound Med. Biol.*, vol. 31, no. 7, pp. 889–894, Jul. 2005.
- [17] B. Widrow and S. Stearns, *Adaptive Signal Processing*. Englewood Cliffs, New Jersey, USA: Prentice Hall, 1985.
- [18] M. E. Anderson, "A 2D Nonlinear Wave Propagation Solver Written in Open-Source MATLAB Code," in *Proceeding IEEE Ultrasonic Symposium*, San Juan, Puerto Rico, Oct. 2000, pp. 1351–1354.
- [19] S. Calle, J.-P. Remenieras, O. Bou Matar, M. Elkateb Hachemi, and F. Patat, "Temporal Analysis of Tissue Displacement Induced by a Transient Ultrasound Radiation Force," *The Journal of the Acoustical Society of America*, vol. 118, no. 5, pp. 2829–2840, nov 2005.
- [20] T. Szabo, *Diagnostic Ultrasound Imaging: Inside Out*. Oxford, UK: Academic Press, 2004, ch. 9 & appendix B.
- [21] C. Greis, "Technology Overview: SonoVue (Bracco, Milan)," *Eur. Radiol. Suppl.*, vol. 14, no. 8, pp. 11–15, Oct. 2004.
- [22] S. M. van der Meer, M. Versluis, D. Lohse, C. T. Chin, A. Bouakaz, and N. de Jong, "The Resonance Frequency of SonoVue(TM) as Observed by High-Speed Optical Imaging," in *Proc. IEEE Ultrason. Symp.*, vol. 1, 2004, pp. 343–345.

- 353 [23] P. Marmottant, S. van der Meer, M. Emmer, M. Versluis, N. de Jong, S. Hilgenfeldt, and D. Lohse, "A Model for Large Amplitude
354 Oscillations of Coated Bubbles Accounting for Buckling and Rupture," *The Journal of the Acoustical Society of America*, vol. 118,
355 no. 6, pp. 3499–3505, Dec. 2005.
- 356 [24] M. S. Plesset, "The Dynamics of Cavitation Bubbles," *Journal of Applied Mechanics*, vol. 16, pp. 277–282, 1949.
- 357 [25] J. M. Gorce, M. Arditì, and M. Schneider, "Influence of bubble size distribution on the echogenicity of ultrasound contrast agents: A
358 study of sonovue." *Investigative radiology*, vol. 35, no. 11, pp. 661–671, Nov 2000.

359 **Sébastien Ménigot** was born in France in 1985. He received his M. Sc. degree in medical imaging technology from the François Rabelais
360 University of Tours, France, in 2008. He obtained his Ph. D. degree in signal processing for medical ultrasound imaging at the François
361 Rabelais University of Tours, France, in 2011. His research focuses on optimal control applied to ultrasound imaging systems.

362 **Jean-Marc Girault** (S'98–M'00) received the Master's degree in "signal processing and biological and medical imaging" from the University
363 of Angers, France, in 1996. He obtained his Ph. D. degree in signal processing in medical ultrasound imaging at the François Rabelais
364 University of Tours, France, in 1999. Finally, he obtained his "Habilitation Diriger les Recherches" (HDR) in signal processing in medical
365 ultrasound imaging at the François Rabelais University of Tours, France, in 2010. He has been a lecturer in signal processing at the University
366 of Tours since 2001. He has written more than fifty scientific communications on medical ultrasound imaging and signal processing. Since
367 2005 he has been the coordinator of the Master's Degree in "medical imaging" at the University François Rabelais of Tours. At the same
368 time, he coordinates the cross-discipline group focusing on "signals, images, imaging" at UMR Inserm-CNRS-University François Rabelais
369 of Tours S930 entitled "Imaging and Brain".

370 **Iulian Voicu** received M. Sc. degree in electronics and telecommunication from the Technical University of Cluj-Napoca, Romania, in 2002.
371 He also obtained his M. Sc. degree in medical imaging from the François Rabelais University, Tours, France, in 2008 and the Ph. D. degree
372 in signal processing for medical ultrasound imaging from the François Rabelais University of Tours, France, in 2011. His research focuses
373 on the development of new signal processing methods to characterize the signal complexity.

374 **Anthony Novell** was born in France in 1983. He received his M. Sc. degree in medical imaging technologies from the François Rabelais
375 University, Tours, France, in 2007. He is currently pursuing his postdoc at the French Institute for Health and Medical Research (Inserm)
376 in Tours, France. His research focuses on contrast agent imaging, capacitive micromachined ultrasonic transducers (cMUTs) and therapeutic
377 ultrasound.

FIGURE CAPTIONS

378

379 **Fig. 1:** Block diagram of adaptive imaging by pulse inversion technique.

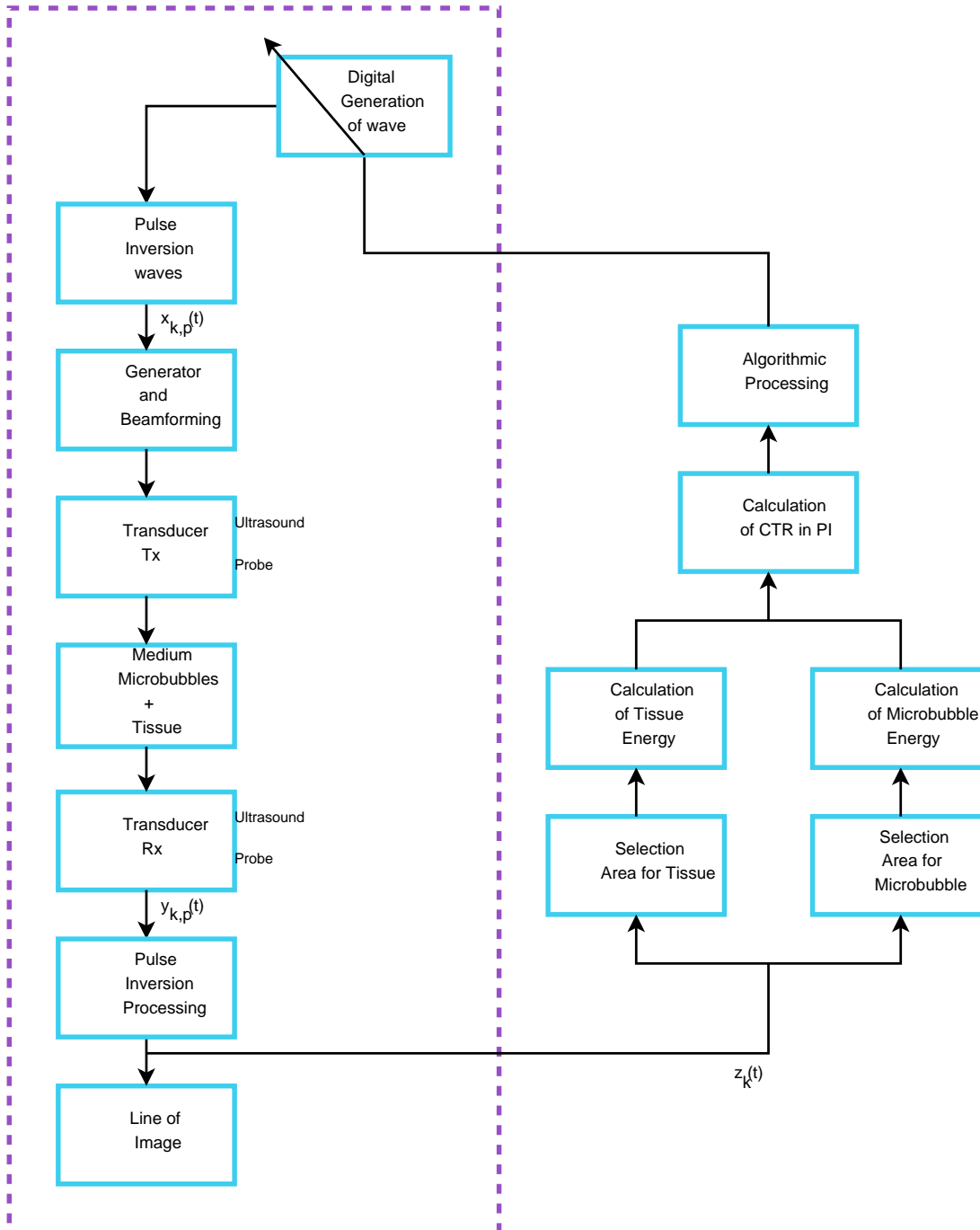
380 **Fig. 2:** Simulation of *CTR* for a transmit frequency of 1 to 4 MHz, a pressure level A_0 of 240 to 400
 381 kPa and a constant number of cycles N_c of 2.3. The simulation included the transducer. Note
 382 that for transmit frequencies above the central frequency of the transducer, the axial resolution
 383 could not be reduced because of the transducer impulse response.

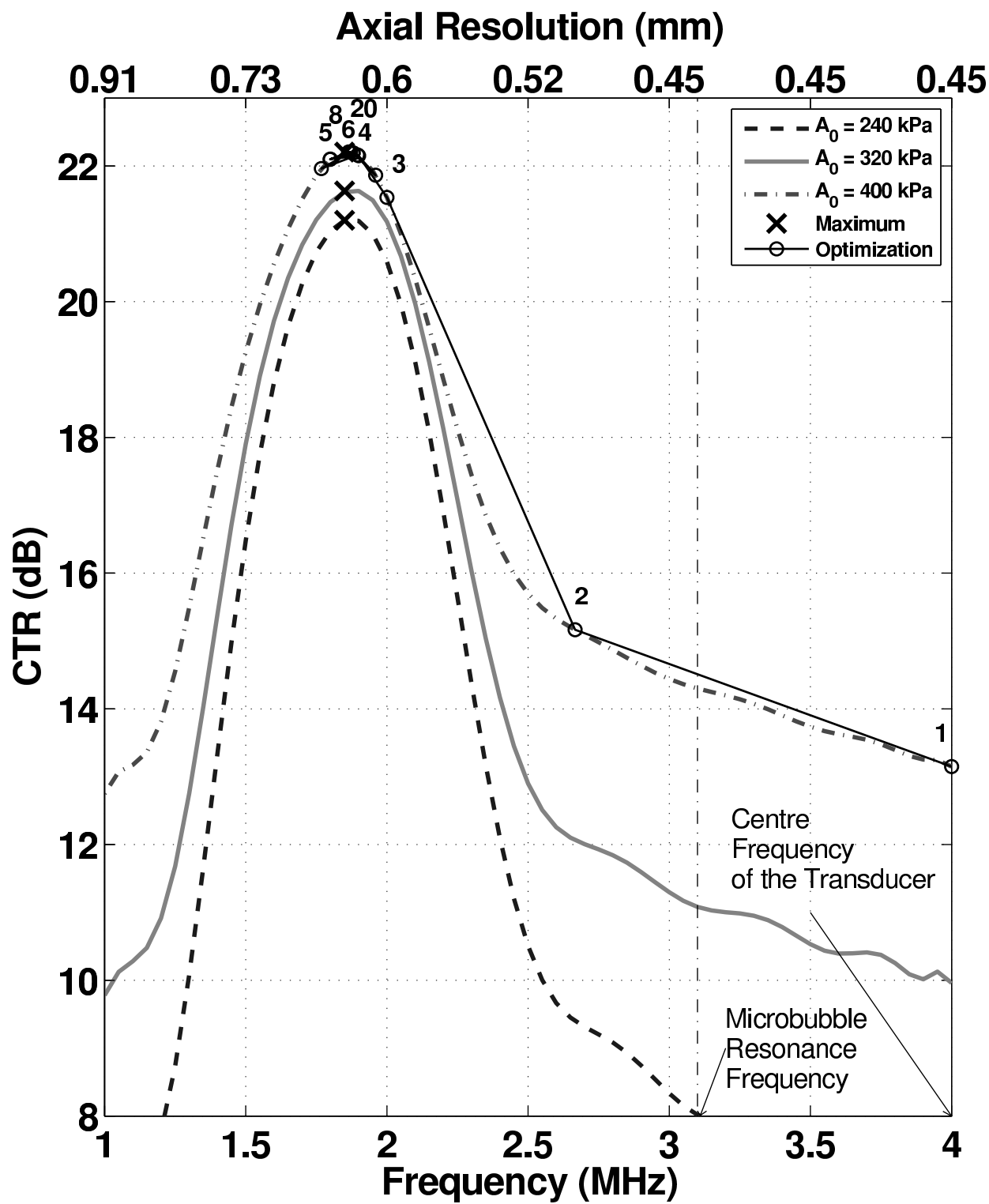
384 **Fig. 3:** Simulation of automatic optimization of the *CTR* by iterative searching for the optimal transmit
 385 frequency for different pressure levels A_0 from 240 to 400 kPa and a constant cycle number N_c
 386 of 2.3. The simulation included the transducer.

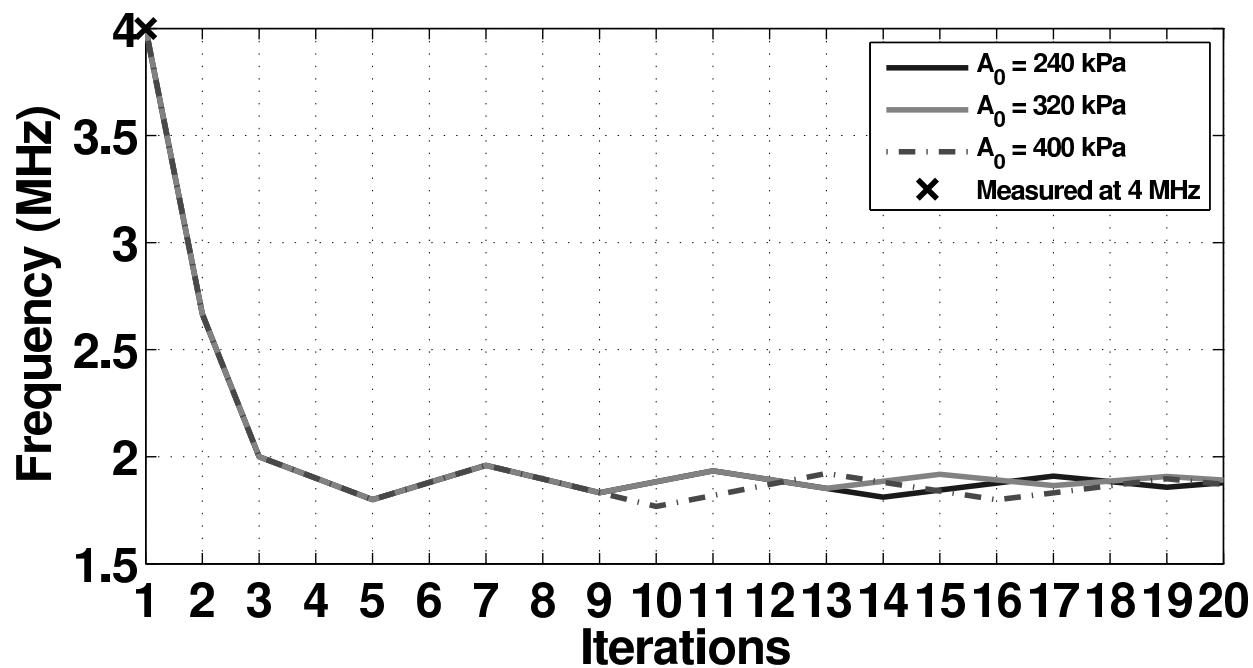
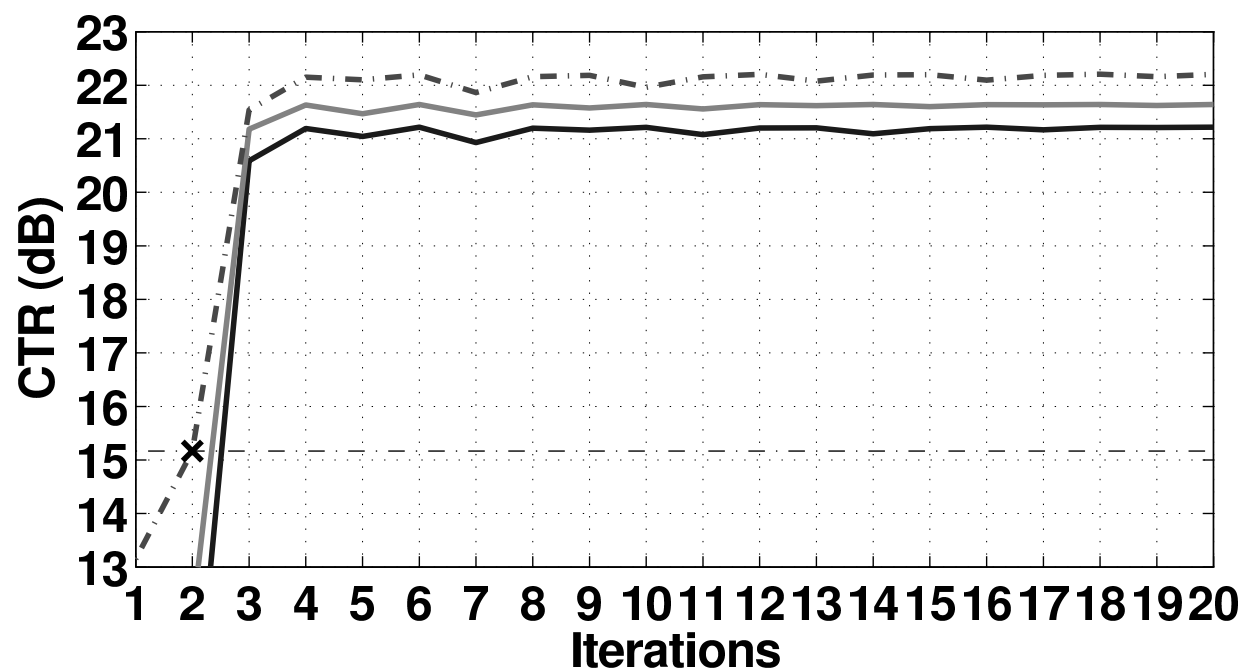
387 **Fig. 4:** Simulation of *CTR* optimization for a pressure level A_0 of 400 kPa and a constant cycle number N_c
 388 of 2.3 in the presence of changing microbubble properties. The first optimization was performed
 389 for a microbubble with a constant radius of $2.5 \mu\text{m}$; the second for a microbubble with a constant
 390 radius of $1.25 \mu\text{m}$. The third optimization began with a microbubble of $2.5 \mu\text{m}$ radius until
 391 iteration 10, the microbubble then changed to $1.25 \mu\text{m}$ radius.

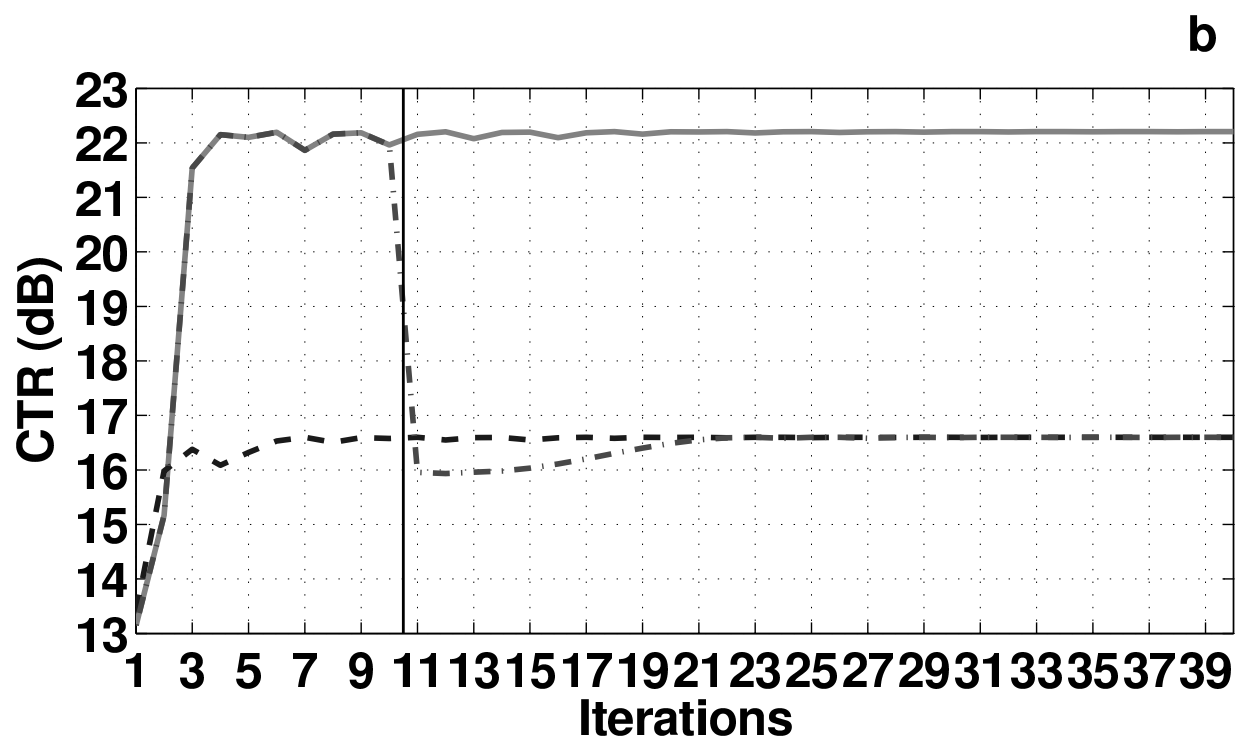
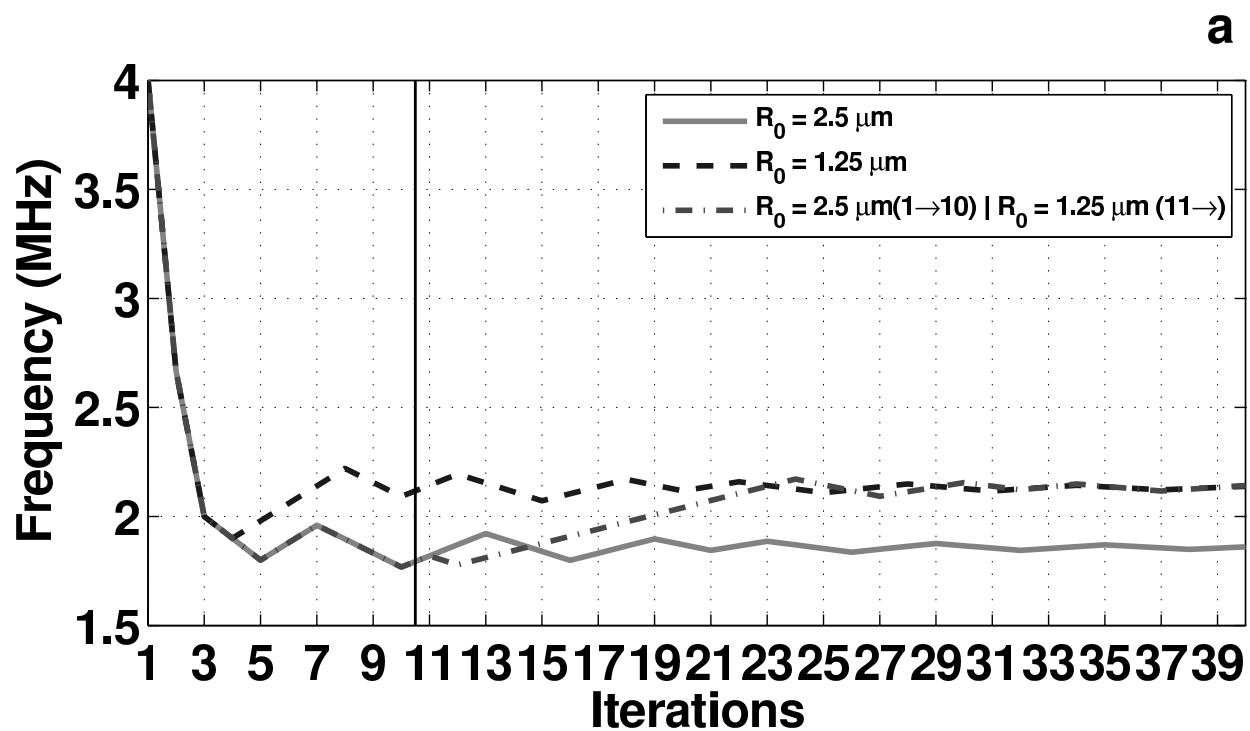
392 **Fig. 5:** Experiment of *CTR* optimization for a pressure level A_0 of 400 kPa at the focal length and a
 393 constant cycle number N_c of 4.

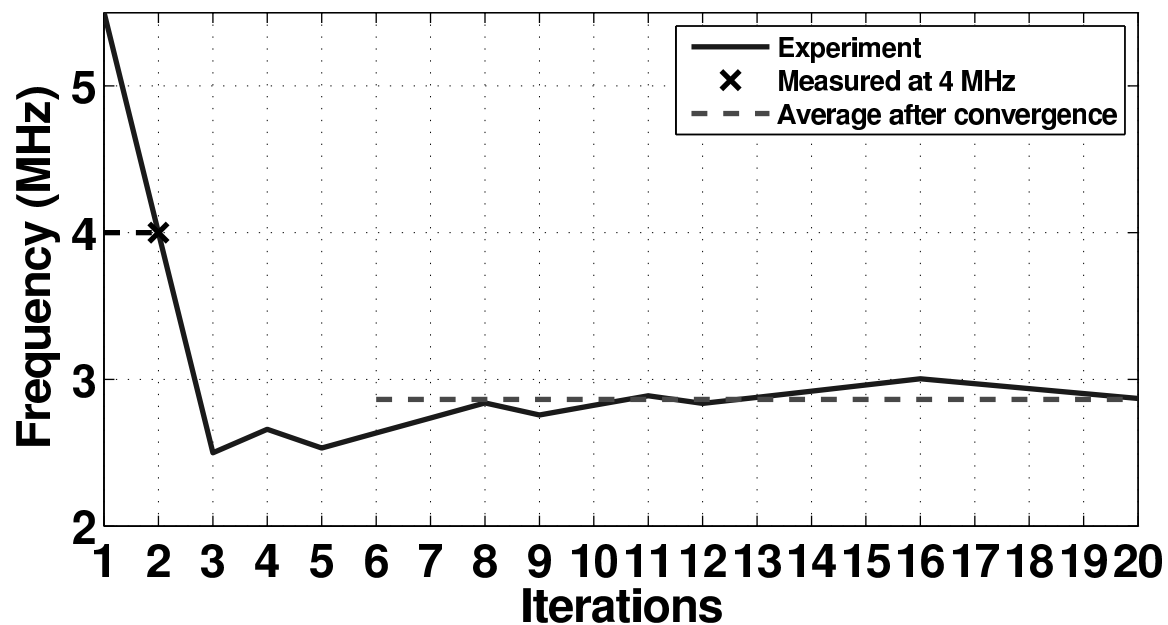
Opened Loop





a**b**



a**b**